Shear-enhanced convection in a mushy layer

JEROME A. NEUFELD[1]† AND J. S. WETTLAUFER[1,2]

[1]Department of Geology and Geophysics, Yale University, New Haven, CT 06520, USA
[2]Department of Physics, Yale University, New Haven, CT 06520, USA

We investigate the effect of an external shear flow on the buoyant instabilities inherent in the directional solidification of a dendritic mushy layer. In the presence of an external shear flow, perturbations of the mush–liquid interface lead to perturbed flow in the bulk fluid that create pressure variations along the mush–liquid interface. These pressure variations drive flow in the mushy layer. A numerical analysis of the stability of the system provides the critical porous-medium Rayleigh number as a function of both the external flow speed and the wavenumber of the interfacial perturbations. In the limit of zero external flow we recover the so-called boundary and mushy layer modes of buoyancy-driven convection first established by Worster (*J. Fluid Mech.*, vol. 237, 1992*b*, p. 649). We find that the application of an external flow can significantly reduce the stability of both the boundary and mushy layer modes. The resultant forced mushy layer mode gives rise to the formation of channels of reduced solid fraction perpendicular to the applied flow that are distinct from the planform found in the absence of an external flow. The stability of the system is examined as a function of the principal thermodynamic and dynamic parameters, and the results are applied to the solidification of sea ice in the presence of vigorous oceanic flow.

1. Introduction

The coupling of natural and imposed fluid flow to phase change can lead to dramatic changes in the morphology of growing crystals that in turn influence the bulk mechanical and electrical properties of the solidified materials (see reviews by Glicksman, Coriell & McFadden 1986; Davis 1990, 2001; Worster 2000). For example, in metallurgical applications, flow within a solidifying network of dendritic crystals, termed a mushy layer, can lead to the formation of zones devoid of solid, called chimneys, which are associated with defects in the resultant material known as 'freckles'. The same class of phenomena occur in a wide range of geophysical problems. For example, convective flows associated with the formation of sea ice dominate the heat and salt fluxes to the ocean that combine to create the high-latitude equivalent of the evaporation–precipitation cycle, and exert a controlling influence on the formation of polar water masses (Wettlaufer, Worster & Huppert 1997; Wells & Wettlaufer 2007). Ultimately, the large-scale wind-driven motion of the sea ice is coupled to its thermodynamic evolution through turbulent boundary layers at the ice–ocean interface (e.g. Morison & McPhee 2001). The coupling of these heat

† Present Address: Institute of Theoretical Geophysics, Department of Applied Mathematics and Theoretical Physics, University of Cambridge, Wilberforce Road, Cambridge CB3 0WA, UK.

and salt fluxes with large-scale oceanic currents is a problem of particular relevance in the light of our analysis here.

Solidification of many geophysical and industrial systems occurs when these multicomponent systems are driven far from thermodynamic equilibrium. The resulting imbalance is relaxed by solidification, through nucleation and settling of crystals or through the morphological instability of planar solid–liquid interfaces (Mullins & Sekerka 1964). In consequence the solid–liquid interface is often highly convoluted and forms an effective porous medium that is thermodynamically reactive, termed a mushy layer. These dendritic arrays have been successfully modelled as a continuum on a scale larger than the inter-dendrite spacing. Within this thermodynamically controlled chemically reactive porous medium, temperature and concentration are coupled through the liquidus relation which describes the solutally dependent freezing point (see reviews by Worster 1992a, 1997, 2000). As the mushy layer solidifies, motion of the interstitial and adjacent fluid can take place owing to buoyancy forces associated with both thermal and compositional gradients. Worster (1992b) and Chen, Lu & Yang (1994) detailed the onset of two distinct modes of convection. A boundary layer mode, associated with the diffusion of solute in the liquid adjacent to the mushy layer, gives rise to convection on a length scale commensurate with compositional diffusion. The stability of this boundary layer mode is largely determined by a compositional Rayleigh number R_C, and leads to fluid motion restricted primarily to the fluid layer. In contrast, a mushy layer mode of convection takes place both within the porous mushy layer and the overlying fluid, giving rise to marked changes in the volume fraction of solid, and hence the permeability in the mushy layer. This mode is triggered when the buoyancy force due to density gradients in the interstitial fluid overcomes the viscous resistive forces associated with the proximity of the crystals. The stability of this mode is characterized by a porous-medium Rayleigh number R_m, which depends on the solid fraction ϕ, and hence the magnitude and structure of the permeability $\Pi(\phi)$, of the dendritic layer. Both modes have been observed in the laboratory (Wettlaufer *et al.* 1997). Because of the dependence of the critical porous-medium Rayleigh number R_m^c on the permeability, we expect forced flows to influence the value of R_m^c and to ultimately result in the formation of regions of zero solid fraction.

The effect of both natural and forced flows on the stability of a solidifying planar solid-liquid interface to the morphological instability first described by Mullins & Sekerka (1964) has been reviewed by Glicksman *et al.* (1986), Davis (1990, 2001) and Worster (2000) and is, in part, motivated by the desire to control material properties influenced by the corrugation of the solid–liquid interface. Of particular relevance to our study is the work of Forth & Wheeler (1989, 1992) who assessed the stability of a planar solid–liquid interface when growth was coupled to a shear flow described by the asymptotic suction profile. They considered the effect of flow on both the diffusive Mullins–Sekerka instability and the convective instability and found travelling wave solutions that propagate in the direction of flow at large wavelengths with a speed proportional to the Reynolds number. Furthermore, they found a slight stabilization of the morphological instability as the magnitude of the external flow is increased.

The interaction of an external flow with the morphology of a mushy layer has been studied previously by Feltham & Worster (1999), Chung & Chen (2001), Feltham *et al.* (2002) and Neufeld *et al.* (2006). In their paper, Feltham & Worster (1999) theoretically evaluated the stability of a mushy layer with a corrugated mush–liquid interface solidifying into an external shear flow. They neglected the effects of buoyancy and found that the coupling between external flow and the corrugated porous medium

produced a Bernoulli pressure variation at the mush–liquid interface that drove flow throughout the underlying mushy layer with a wavelength commensurate with the mushy layer depth. This flow in turn perturbed the isotherms within the mushy layer giving rise to enhanced growth of the interfacial corrugations of the mush–liquid interface. A more detailed study including both the effect of an external flow and buoyant forcing due to thermal and compositional gradients was later undertaken by Chung & Chen (2001) who coupled flow, described by an asymptotic suction profile, to both the thermal and compositional profiles across the perturbed mush–liquid interface. The fluid velocity at the corrugated mush–liquid interface was treated using a Beavers–Joseph boundary condition (Beavers & Joseph 1967). Additionally, they considered perturbations to both the thermal and solutal fields, using the material parameters of a 28 wt% aqueous ammonium chloride solution. They argued that the coupling of the external flow to the corrugated mush–liquid interface leads to a new forced mode of instability and that if perturbations to both the thermal and compositional fields are considered, this mode can become forced at shear rates substantially smaller than those found by Feltham & Worster (1999). However, in contrast to the work of Feltham & Worster (1999) this new forced mode had a wavelength commensurate with the boundary layer mode.

In the present paper, we study the effect of an external shear flow on the stability of the mushy layer system to buoyancy-driven convection. In §2 we outline the physical configuration and detail the mathematical formulation of the problem. We then review the unperturbed state in §3, and formulate the linear stability analysis and our solution procedure in §4. Finally, in §5 we explore the effect of the external flow and dynamic and thermodynamic parameters on the convective modes of the system and describe the physical basis of this interaction. We then put our remarks into the context of previous studies. Concluding remarks are made in §6.

2. Governing equations

Following previous studies, reviewed most recently by Worster (1997, 2000), we consider a mushy layer, bounded from below by a horizontal plane defined by the eutectic temperature T_E, which is solidified at constant rate V into an overlying liquid of bulk concentration C_0 and temperature T_∞ with a far-field velocity of $\boldsymbol{u} = U_\infty \hat{\boldsymbol{x}}$ (see figure 1). Because of the large interfacial surface area within the mushy layer we assume that the temperature and concentration of the interstitial liquid are coupled through the liquidus condition which we approximate by the linear relationship $T_L(C) = T_E + \Gamma(C - C_E)$ where C_E is the eutectic concentration and Γ is the liquidus slope. Here we have considered solidification of a super-eutectic binary solution such as a super-eutectic aqueous ammonium chloride solution. Length, time and pressure scales within the system are given by κ/V, κ/V^2 and $\beta^* \Delta C \rho_0 g \kappa / V$ respectively. Here ρ_0 is the reference density, g is the acceleration due to gravity, $\Delta C = C_0 - C_E$ is the compositional scale, κ is the thermal diffusivity and $\beta^* \equiv \tilde{\beta} - \Gamma \tilde{\alpha}$, where $\tilde{\alpha}$ and $\tilde{\beta}$ are the thermal and solutal expansion coefficients respectively. Finally, we define the non-dimensional temperature θ and composition Θ as

$$\theta = \frac{T - T_L(C_0)}{\Delta T} \quad \text{and} \quad \Theta = \frac{C - C_0}{\Delta C},$$

where $\Delta T = \Gamma \Delta C = T_L(C_0) - T_E$, and hence the thermal (ΔT) and compositional (ΔC) scales are representative of the variations over the depth of the mushy layer.
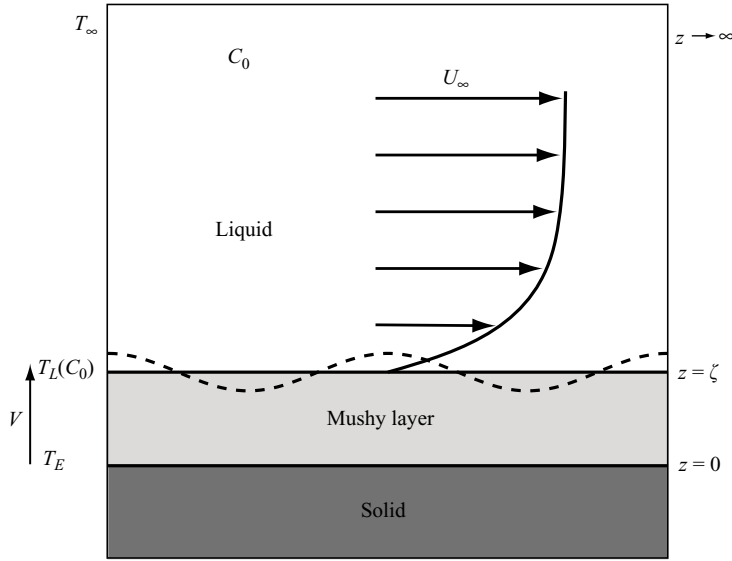
FIGURE 1. Schematic of the system under consideration. A uniform shear flow is imposed over a growing mushy layer. Flow within the mushy layer is coupled to that in the liquid via a perturbed mush–liquid interface indicated by the dotted line.

2.1. *Equations in the liquid*

The interface between the mushy layer and the liquid is defined by $z = \zeta(x, t)$. The equations governing heat, solute and momentum in the liquid region $(z > \zeta)$ are

$$(\partial_t - \partial_z)\theta + \boldsymbol{u} \cdot \nabla\theta = \nabla^2\theta, \tag{2.1}$$

$$(\partial_t - \partial_z)\Theta + \boldsymbol{u} \cdot \nabla\Theta = \epsilon\nabla^2\Theta, \tag{2.2}$$

$$(\partial_t - \partial_z)\boldsymbol{u} + \boldsymbol{u} \cdot \nabla\boldsymbol{u} = -PrR_C \frac{\beta^*}{\tilde{\beta}}\nabla p + Pr\nabla^2\boldsymbol{u} + Pr(R_T\theta - R_C\Theta)\hat{\boldsymbol{z}}, \tag{2.3}$$

$$\nabla \cdot \boldsymbol{u} = 0, \tag{2.4}$$

where $\epsilon = D/\kappa$ is the inverse Lewis number which is the ratio of solutal to thermal diffusivity and $Pr = \nu/\kappa$ is the Prandtl number, where ν is the kinematic viscosity of the fluid. Finally, the thermal and solutal Rayleigh numbers are defined as

$$R_T = \frac{g\tilde{\alpha}\Delta T(\kappa/V)^3}{\kappa\nu} \quad \text{and} \quad R_C = \frac{g\tilde{\beta}\Delta C(\kappa/V)^3}{\kappa\nu}$$

respectively.

2.2. *Equations in the mushy layer*

As described above, the mushy layer is a dendritic array of crystals the interstices of which are filled with a fluid that has a composition determined by the local temperature through the liquidus relationship as described by Hills, Loper & Roberts (1983) and Worster (1986, 2000). We utilize a continuum model known as 'ideal mushy layer theory' in which differences in density, specific heat and thermal conductivity between liquid and solid phases are neglected. This model is homogenized on a length scale that is large relative to the dendrite spacing, but small relative to the thermal length scale of the system. The equations governing heat and solute in the mushy

layer ($0 < z < \zeta$) are written as

$$(\partial_t - \partial_z)(\theta - \mathscr{S}\phi) + \boldsymbol{u} \cdot \nabla\theta = \nabla^2\theta, \tag{2.5}$$

$$(\partial_t - \partial_z)[(1 - \phi)\theta + \mathscr{C}\phi] + \boldsymbol{u} \cdot \nabla\theta = 0, \tag{2.6}$$

where ϕ is the local volume fraction of solid within the mushy layer as described in §1. Since diffusion of solute occurs only within the fluid on the length scale of the fluid interstices we neglect the effects of compositional diffusion within the mushy layer. In consequence, there are two dimensionless parameters introduced. The Stefan number,

$$\mathscr{S} = \frac{\mathscr{L}}{c\Delta T},$$

captures the relative influence of the heat of fusion to the specific heat and is defined in terms of the latent heat of fusion $\mathscr{L}$, and the specific heat c. The concentration ratio,

$$\mathscr{C} = \frac{C_s - C_0}{\Delta C},$$

characterizes the quantity of solute exchanged locally upon solidification and dissolution, and is defined in terms of the concentration of solute within the solid C_s. Within the mushy layer we assume that the interstitial fluid is incompressible and hence, when combined with the assumption that $\rho_s = \rho_l$, continuity is expressed by

$$\nabla \cdot \boldsymbol{u} = 0. \tag{2.7}$$

Conservation of momentum is treated using Darcy's equation

$$\boldsymbol{u} = -R_m \Pi_1(\phi)(\nabla p + \theta \hat{\boldsymbol{z}}), \tag{2.8}$$

where p is the dynamic pressure. The permeability is expressed as $\Pi = \tilde{\Pi}_0 \Pi_1(\phi)$, and thus a porous-medium Rayleigh number, described above, can be defined as

$$R_m \equiv \frac{g\beta^* \Delta C \tilde{\Pi}_0 (\kappa/V)}{\kappa \nu}.$$

Finally, the Darcy number

$$\Pi_0 \equiv \frac{\tilde{\Pi}_0}{(\kappa/V)^2}$$

is a non-dimensional measure of the permeability of the system. As we shall see later the Darcy number is the parameter with the greatest influence on the stability of the mushy layer to a mode forced by shear flow in the adjacent liquid.

2.3. *Boundary conditions*

The mushy layer is bounded from below by the eutectic ($z = 0$) where

$$\theta = -1 \quad \text{and} \quad w = 0. \tag{2.9a, b}$$

At the mush–liquid interface ($z = \zeta$) we impose continuity of the thermal and solute fields. We conserve heat at the interface, as expressed by the Stefan condition, and follow Worster (1986, 2000) in using the assumption of marginal equilibrium, which states that the liquid has the minimal interfacial temperature gradient necessary to eliminate constitutional supercooling. This assumption also constrains the solid fraction. Velocity normal to the interface and pressure are continuous across the

mush–liquid interface and a no-slip condition is applied. These boundary conditions are expressed as

$$[\theta]_l^m = 0, \quad \theta^l = \Theta^l, \quad \phi = 0, \qquad (2.10a,b,c)$$

$$\phi \mathscr{S} v_n = [\hat{\boldsymbol{n}} \cdot \nabla \theta]_l^m, \quad [\hat{\boldsymbol{n}} \cdot \nabla \theta]_l = [\hat{\boldsymbol{n}} \cdot \nabla \Theta]_l, \qquad (2.10d,e)$$

$$[\boldsymbol{u} \cdot \hat{\boldsymbol{n}}]_l^m = 0, \quad [p]_l^m = 0, \quad [\boldsymbol{u} \times \hat{\boldsymbol{n}}]_l = 0, \qquad (2.10f,g,h)$$

respectively, where v_n is the normal velocity of the interface. Finally, as $z \to \infty$ the temperature, composition and velocity asymptote to their far-field values:

$$\theta \to \theta_\infty, \quad \Theta \to 0, \quad \boldsymbol{u} \to U_\infty \hat{\boldsymbol{x}}. \qquad (2.11a,b,c)$$

3. Steady-state solution

The governing equations and boundary conditions admit a steady-state solution similar to that presented by Worster (1992b), Feltham & Worster (1999) and Chung & Chen (2001) and are reviewed here to ensure a relatively self-contained treatment. In this steady state, temperature and composition depend only on the vertical coordinate and there is no flow within the mushy layer, $\boldsymbol{u}_0^m = 0$.

In the overlying liquid the steady-state temperature θ_0, concentration Θ_0 and horizontal velocity u_0, all decay to their far-field values with length scales set by the thermal and solutal diffusivities and viscosity respectively:

$$\theta_0(z) = \theta_\infty + (\theta_i - \theta_\infty) e^{-(z-\zeta_0)}, \qquad (3.1)$$

$$\Theta_0(z) = \theta_i e^{-(z-\zeta_0)/\epsilon}, \qquad (3.2)$$

$$u_0(z) = U_\infty \left[1 - e^{-(z-\zeta_0)/Pr}\right]. \qquad (3.3)$$

It is immediately clear that there are three length scales of increasing thickness associated with compositional, thermal and viscous effects, which give rise to three nested boundary layers. The interfacial temperature and concentration, θ_i, derived from the condition of marginal stability, are given by

$$\theta_i = -\frac{\epsilon}{1-\epsilon}\theta_\infty. \qquad (3.4)$$

In the mushy layer temperature and concentration are constrained to each other by the liquidus relation and are given implicitly by the transcendental equation

$$z = \frac{\alpha - \mathscr{C}}{\alpha - \beta} \ln\left(\frac{\alpha+1}{\alpha-\theta_0}\right) + \frac{\mathscr{C} - \beta}{\alpha - \beta} \ln\left(\frac{\beta+1}{\beta-\theta_0}\right), \qquad (3.5)$$

where

$$\alpha, \beta \equiv \frac{1}{2}(\mathscr{S} + \mathscr{C} + \theta_\infty) \pm \frac{1}{2}\sqrt{(\mathscr{S} + \mathscr{C} + \theta_\infty)^2 - 4(\mathscr{S}\theta_i + \mathscr{C}\theta_\infty)}.$$

Finally, the steady-state solid fraction is given by

$$\phi_0 = \frac{\theta_i - \theta_0}{\mathscr{C} - \theta_0}. \qquad (3.6)$$

4. Marginal stability analysis

We consider perturbations to the field variables of typical normal mode form

$$(\theta, \Theta, \phi, \Omega, u, w, \zeta) = (\theta_1, \Theta_1, \phi_1, \Omega_1, u_1, w_1, \zeta_1) e^{\sigma t + i(k_x x + k_y y)}, \qquad (4.1)$$

such that $\sigma = \sigma_r + i\sigma_i$ is the complex growth rate and k_x and k_y are the wavenumbers of perturbations in the $\hat{x}$- and $\hat{y}$-directions respectively. As shown in the analysis of Chung & Chen (2001), Squire's transformation can be used to define an equivalent two-dimensional problem. The two-dimensional problem is characterized by a horizontal wavenumber $k = \sqrt{k_x^2 + k_y^2}$ and an effective shear flow velocity

$$\tilde{u}_0 = \frac{k_x}{k} u_0 = \frac{k_x U_\infty}{\sqrt{k_x^2 + k_y^2}} \left[1 - e^{-(z - \zeta_0)/Pr} \right], \qquad (4.2)$$

in which the external shear flow is in the $\hat{x}$-direction. Alternatively, this can be written as

$$\tilde{u}_0 = u_0 \cos(\vartheta_k) \qquad (4.3)$$

where ϑ_k is the angle between the perturbation and the imposed flow. The immediate implication of Squire's transformation is therefore that the applied external flow has greatest influence on longitudinal modes while leaving the stability of transverse modes unchanged. Therefore, in the following analysis we consider perturbations to the basic steady-state in the $\hat{x}$-direction only and interpret the resultant eigenfunctions accordingly. The perturbation equations in the overlying liquid region ($\zeta_0 < z < \infty$) can be defined in terms of $\Omega_1 \equiv ik(ikw_1 - Du_1)$, and are written as

$$(D^2 + D - k^2 - i\sigma_i)\theta_1 = iku_0\theta_1 + w_1 D\theta_0, \qquad (4.4)$$

$$(\epsilon D^2 + D - \epsilon k^2 - i\sigma_i)\Theta_1 = iku_0\Theta_1 + w_1 D\Theta_0, \qquad (4.5)$$

$$(PrD^2 + D - Prk^2 - i\sigma_i)\Omega_1 = ik(u_0\Omega_1 - w_1 D^2 u_0) + k^2 Pr(R_T\theta_1 - R_C\Theta_1), \qquad (4.6)$$

$$(D^2 - k^2)w_1 = \Omega_1, \qquad (4.7)$$

where $D \equiv d/dz$.

The perturbation equations in the mushy layer ($0 < z < \zeta_0$) are

$$(D^2 + D - k^2 - i\sigma_i)\theta_1 = \mathscr{S}(D - i\sigma_i)\phi_1 + w_1 D\theta_0, \qquad (4.8)$$

$$(\mathscr{C} - \theta_0)(D - i\sigma_i)\phi_1 + (1 - \phi_0)(D - i\sigma_i)\theta_1 = \theta_1 D\phi_0 + \phi_1 D\theta_0 + w_1 D\theta_0, \qquad (4.9)$$

$$\left[D^2 - \frac{D\Pi_1(\phi)}{\Pi_1(\phi)} D - k^2 \right] w_1 = k^2 R_m \Pi_1(\phi)\theta_1. \qquad (4.10)$$

Boundary conditions applied to the perturbation equations are as follows. Perturbations to the solid–mush interfacial position at the eutectic ($z = 0$) are not expected to play a dominant role in the development of forced or convective instability and so we write the perturbed boundary condition at the eutectic as

$$\theta_1^m = 0 \quad \text{and} \quad w_1^m = 0. \qquad (4.11a, b)$$

At the mush–liquid interface the perturbation boundary conditions are

$$[\theta_1 + \zeta_1 D\theta_0]_l^m = 0, \quad [\theta_1 + \zeta_1 D\theta_0]_l = [\Theta_1 + \zeta_1 D\Theta_0]_l, \qquad (4.12a, b)$$

$$\phi_1 + \zeta_1 D\phi_0 = 0, \quad [w_1]_l^m = 0, \qquad (4.12c, d)$$

$$[Dw_1]_m = -\frac{\Pi_0 \Pi_1(\phi)}{Pr} [PrD\Omega_1 - i\sigma_i Dw_1 + \Omega_1 + (k^2 + ikU_\infty/Pr)w_1]_l, \qquad (4.12e)$$

$$[Dw_1 - ikDu_0\zeta_1]_l = 0, \quad [D\theta_1 + \zeta_1 D^2\theta_0]_l^m = 0, \qquad (4.12f, g)$$

$$[D\theta_1 + \zeta_1 D^2\theta_0]_l = [D\Theta_1 + \zeta_1 D^2\Theta_0]_l, \qquad (4.12h)$$

where boundary condition (4.12e) derives from pressure continuity across the interface, $[p]_l^m = 0$. Finally, in the far field $(z \to \infty)$

$$\theta_1^l \to 0, \quad \Theta_1^l \to 0, \quad \Omega_1^l \to 0, \quad w_1^l \to 0. \qquad (4.13a, b, c, d)$$

4.1. *Perturbation equations on the finite domain $(S, s) = [0, 1]$*

The perturbation equations are rewritten with the steady-state thermal field as the independent variable in the manner suggested by Worster (1997). This procedure avoids inversion of the transcendental equation for the steady-state temperature in the mushy layer, and maps the mushy layer $(z \to S)$ and the infinite half-space of the liquid $(z \to s)$ onto the single domain $(S, s) = [0, 1]$. Thus, the problem can be posed as a system of thirteen coupled ordinary differential equations plus a free boundary with fourteen associated boundary conditions, where the boundary conditions on perturbations in the liquid are matched to the asymptotic values detailed in the Appendix.

In terms of the independent variable

$$s = \frac{\theta_\infty - \theta_0}{\theta_\infty - \theta_i} = e^{-(z - \zeta_0)}$$

the vertical derivatives become

$$D = -sD_s \quad \text{and} \quad D^2 = s^2 D_s^2 + sD_s,$$

where $D_s \equiv d/ds$, and hence the perturbation equations (4.4)–(4.7) become

$$\left(s^2 D_s^2 - k^2 - i\sigma_i\right)\theta_1 = ikU_\infty\left(1 - s^{1/Pr}\right)\theta_1 + (\theta_\infty - \theta_i)sw_1, \qquad (4.14)$$

$$\left(\epsilon s^2 D_s^2 + (\epsilon - 1)sD_s - \epsilon k^2 - i\sigma_i\right)\Theta_1 = ikU_\infty\left(1 - s^{1/Pr}\right)\Theta_1 - (\theta_i/\epsilon)s^{1/\epsilon}w_1, \qquad (4.15)$$

$$\left(Pr s^2 D_s^2 + (Pr - 1)sD_s - Pr k^2 - i\sigma_i\right)\Omega_1$$
$$= ikU_\infty\left[\left(1 - s^{1/Pr}\right)\Omega_1 + Pr^{-2}s^{1/Pr}w_1\right] + k^2 Pr(R_T\theta_1 - R_C\Theta_1), \qquad (4.16)$$

$$\left(s^2 D_s^2 + sD_s - k^2\right)w_1 = \Omega_1. \qquad (4.17)$$

Within the mushy layer the perturbation equations are rewritten in terms of

$$S = \frac{1 + \theta_0}{1 + \theta_i}.$$

To simplify our notation we define $\Lambda = (1 + \theta_i)^{-1}$ and rewrite the vertical derivatives as

$$D = \Lambda D\theta_0 D_S \quad \text{and} \quad D^2 = \Lambda^2 (D\theta_0)^2 D_S^2 - [1 + \mathscr{S}(\mathscr{C} - \theta_i)/(\mathscr{C} - \theta_0)^2]\Lambda D\theta_0 D_S.$$

Under this transformation the perturbation equations in the mushy layer become

$$\left[\Lambda^2(D\theta_0)^2 D_S^2 - \frac{\mathscr{S}(\mathscr{C} - \theta_i)}{(\mathscr{C} - \theta_0)^2}\Lambda D\theta_0 D_S - k^2 - i\sigma_i\right]\theta_1 = \mathscr{S}(\Lambda D\theta_0 D_S - i\sigma_i)\phi_1 + w_1 D\theta_0, \qquad (4.18)$$

$$(\mathscr{C} - \theta_0)(\Lambda D\theta_0 D_S - i\sigma_i)\phi_1 + \left(\frac{\mathscr{C} - \theta_i}{\mathscr{C} - \theta_0}\right)(\Lambda D\theta_0 D_S - i\sigma_i)\theta_1$$
$$= \left[\frac{\theta_i - \mathscr{C}}{(\mathscr{C} - \theta_0)^2}\theta_1 + \phi_1 + w_1\right]D\theta_0, \qquad (4.19)$$

$$\left\{ \Lambda^2(\mathrm{D}\theta_0)^2 D_S^2 - \left[1 + \frac{\mathscr{S}(\mathscr{C} - \theta_i)}{(\mathscr{C} - \theta_0)^2} + \frac{\Lambda \mathrm{D}\theta_0 D_S \Pi_1(\phi)}{\Pi_1(\phi)} \right] \Lambda \mathrm{D}\theta_0 D_S - k^2 \right\} w_1$$
$$= k^2 R_m \Pi_1(\phi)\theta_1. \quad (4.20)$$

The boundary conditions can be similarly transformed. At the eutectic point $(S = 0)$ we find

$$\theta_1^m = 0 \quad \text{and} \quad w_1^m = 0. \quad (4.21a,b)$$

The boundary conditions at the mush–liquid interface $(s = S = 1)$ become

$$\theta_1^l = \theta_1^m, \quad \theta_1^l = \Theta_1^l, \quad (4.22a,b)$$

$$\phi_1 = \zeta_1 \left(\frac{\theta_\infty - \theta_i}{\mathscr{C} - \theta_i} \right), \quad w_1^l = w_1^m, \quad (4.22c,d)$$

$$\Lambda(\theta_\infty - \theta_i)D_S w_1^m = -\frac{\Pi_0 \Pi_1(\phi)}{Pr}[-Pr\mathrm{D}_s\Omega_1 + \Omega_1 + \mathrm{i}\sigma_i \mathrm{D}_s w_1 + (k^2 + \mathrm{i}kU_\infty/Pr)w_1]_l, \quad (4.22e)$$

$$\mathrm{D}_s w_1^l = -\mathrm{i}kU_\infty \zeta_1/Pr, \quad (4.22f)$$

$$\Lambda(\theta_\infty - \theta_i)D_S \theta_1^m + \mathrm{D}_S \theta_1^l = \mathscr{S}\zeta_1 \left(\frac{\theta_\infty - \theta_i}{\mathscr{C} - \theta_i} \right), \quad (4.22g)$$

$$\zeta_1 = \frac{\epsilon}{\theta_\infty}[\mathrm{D}_s\theta_1 - \mathrm{D}_s\Theta_1]_l. \quad (4.22h)$$

The far-field boundary conditions in the liquid, $(4.13a{-}d)$, now written in the s domain have a regular singularity at $s = 0$. We therefore recast the far-field boundary conditions in terms of matching conditions with the asymptotic behaviour derived from analytic solutions to the reduced perturbation equations for $s \ll 1$. These asymptotic conditions are detailed in the Appendix.

The perturbation equations and associated boundary conditions are solved using a multiple shooting technique with orthonormalization as detailed in Acher, Mattheij & Russell (1987) and Keller (1976). Integration is initiated with the asymptotic relations in the liquid, and with the boundary values at the eutectic within the mushy layer. These equations are then integrated over the s and S domains using the orthonormalization technique at points fixed *a priori*. Powell's method, as detailed by Press *et al.* (1997), is then used to reduce the mismatch in boundary conditions at $s = S = 1$, thereby providing the eigenvalues and eigenfunctions of the problem.

5. Results and discussion

5.1. *The effect of an external flow*

We begin this section by noting that the breadth of the parameter space forces us to engage in a strategic, physically motivated, exploration of the stability of the system. We first consider the case of all three thermodynamic parameters $\mathscr{C} = \mathscr{S} = \theta_\infty = 1$, with $Pr = 10$ and $\Pi_0 = 10^{-5}$. We write

$$R_c = \frac{\tilde{\beta}}{\beta^\star \Pi_0} R_m \quad (5.1)$$

and take $R_T = 0$ to reflect the fact that composition dominates the equation of state and hence thermal convection plays a secondary role. This substantially simplifies the resultant stability diagram while capturing the principal modes of compositionally
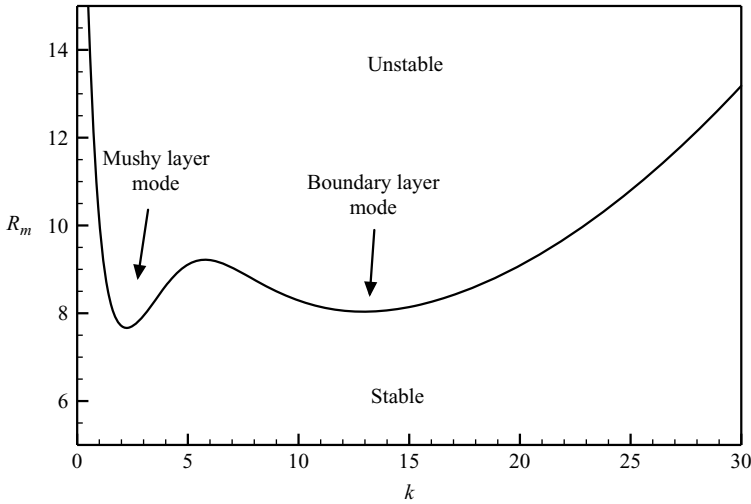
FIGURE 2. Neutral stability curve for $\mathcal{S} = \mathcal{C} = \theta_\infty = 1$, $\Pi_0 = 10^{-5}$ and $U_\infty = 0$. In the limit $U_\infty = 0$ we recover the result of Worster (1992*b*) with the associated boundary layer ($k \simeq 13$) and mushy layer ($k \simeq 2.5$) modes.
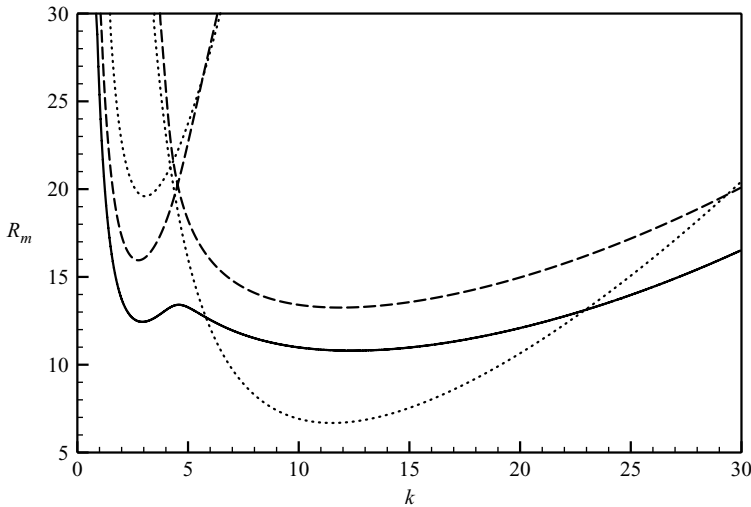

FIGURE 3. Critical Rayleigh number for increasing U_∞. Parameter values are $\mathcal{C} = \mathcal{S} = \theta_\infty = 1$ and $\Pi_0 = 10^{-5}$. Neutral stability curves are $U_\infty = 500$ (solid), $U_\infty = 1000$ (dashed) and $U_\infty = 4000$ (dotted).

dominated convection. We demonstrate this by setting $U_\infty = 0$ to capture the two direct modes of instability shown in figure 2 that we can readily identify as the two modes first characterized by Worster (1992*b*): a short-wavelength (large-wavenumber) boundary layer mode and a long-wavelength (small-wavenumber) mode termed the mushy layer mode. These stationary modes arise from unstable stratification in the diffusional boundary layer ahead of the mushy layer and of the fluid within the interstices of the mushy layer respectively, as described briefly in the introduction.

By holding the parameters $\mathcal{C} = \mathcal{S} = \theta_\infty = 1$ and $\Pi_0 = 10^{-5}$ constant and increasing the strength of the external shear flow we can ascertain the effect of the external flow on the stability of the system as shown in figures 3 and 4. The application of the
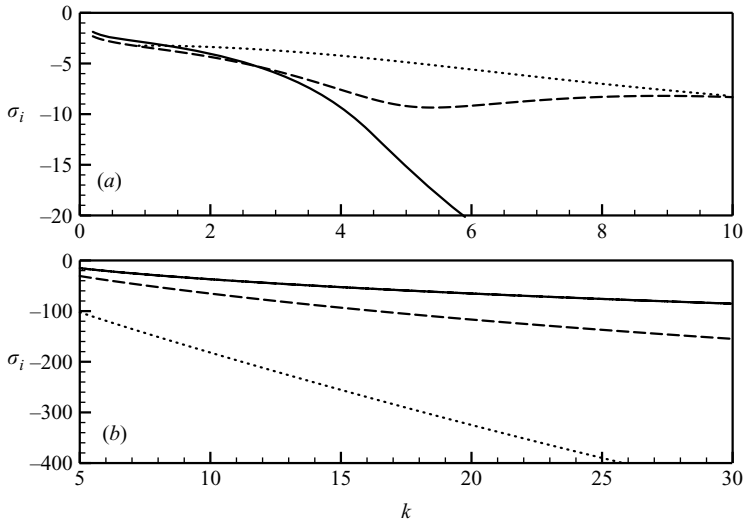
FIGURE 4. Complex growth rate shown as a function of the wavenumber for (*a*) the mushy layer mode and (*b*) the boundary layer mode (note the differing scales for boundary and mushy layer complex growth rates). The curves are for $U_\infty = 500$ (solid), $U_\infty = 1000$ (dashed) and $U_\infty = 4000$ (dotted) and are all shown for $\mathscr{C} = \mathscr{S} = \theta_\infty = 1$ and $\Pi_0 = 10^{-5}$.
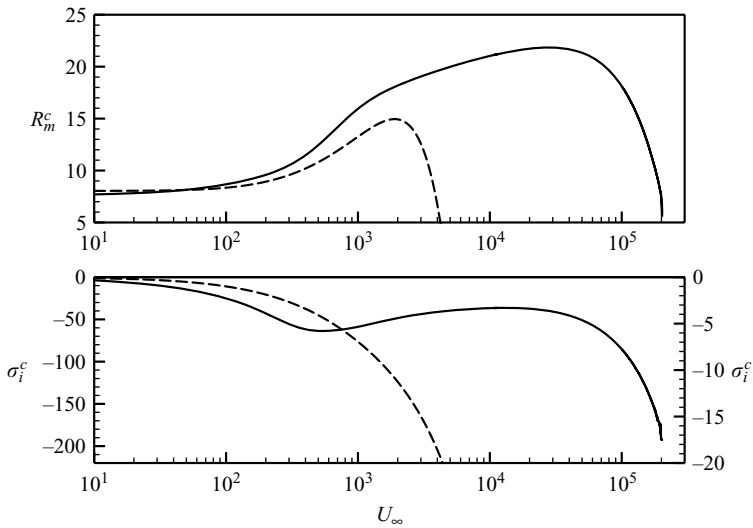

FIGURE 5. The variation of the critical Rayleigh number R_m^c and complex growth rate σ_i^c associated with the boundary (dashed, left-hand axis) and mushy layer (solid, right-hand axis) modes of convection as a function of the external flow speed U_∞.

external flow breaks the symmetry of buoyancy-driven convection thereby creating travelling wave solutions for both the boundary and mushy layer modes. Moreover, as U_∞ is increased the wave speed of the boundary layer mode increases to values greatly in excess of that of the mushy layer mode, thereby separating the two modes as shown in figure 4.

The overall effect of the external flow on both the boundary and mushy layer modes is nicely characterized by plotting the minimum critical Rayleigh number of each mode, $R_m^c = R_m^c(U_\infty)$ as shown in figure 5. We see that for both modes, increasing

the magnitude of the external flow first causes a minor increase in the stability of the system. Then, as the external flow is increased beyond a critical value there is a dramatic decrease in the stability of the system. As is clear from figure 5 the critical flow rate for the boundary layer mode is much less than that for the mushy layer mode, and in both cases is dependent upon, among other things, the thermodynamic parameters of the system and the permeability of the mushy layer.

5.2. *Physical mechanisms*

Now we discuss the physical mechanisms underlying the behaviour of the curves of R_m^c with respect to the magnitude of the external flow. Importantly, we note that the imposition of a weak external flow modifies the pre-existing buoyant modes of convection while a vigorous external flow drives instabilities which arise from the interaction of the external flow with a deformable interface. In both cases, the presence of an external flow breaks the symmetry of the system resulting in $\sigma_i \neq 0$. Thus both the boundary and mushy layer modes admit travelling wave solutions that propagate in the direction of the imposed flow. These two modes are illustrated in figures 6 and 7 and for both modes the influence on the stability of the system can be most readily understood by examining the secondary flow generated as the external flow impinges upon the corrugated mush–liquid interface.

In the absence of an external flow, secondary fluid motions are driven by density differences, primarily due to compositional gradients, both within the compositional boundary layer and within the interstices of the mushy layer. The nature of this buoyancy-driven flow has been previously demonstrated by Worster (1992*b*) for both the mushy layer and boundary layer modes and is characterized by upwellings above the peaks and downwellings above the troughs of the interface. We find that these patterns of buoyancy-driven convection are progressively modified as the strength of the external flow is increased. For sufficiently vigourous external flows the secondary flow is dominated by interactions of the external flow with the corrugated mush–liquid interface. In this limit, because the no-slip condition must be satisfied all along the corrugated mush-liquid interface, the presence of the peaks (troughs) effectively reduces (enhances) the flow speed further into (recessed from) the bulk fluid relative to the unperturbed planar state. The result is retrograde motion at the peaks and prograde motion at the troughs (with respect to the bulk flow). Continuity requires that these motions be balanced by upwellings on the upstream face of the peaks and downwellings on the downstream face of the peaks with a phase difference of nearly $\pi/2$ (the phase difference becoming exactly $\pi/2$ only in the limit of a non-deformable corrugated interface).

The principal effect of a weak external flow (small U_∞) on the convective modes of instability is to break the symmetry of the unforced problem. Advection of both the thermal and solutal fields by the secondary flow introduces a space phase shift in the growth drive along the interface leading to travelling wave solutions. In addition, as U_∞ is increased the influence of the corrugated interface becomes more pronounced and the associated secondary flow leads to lateral advection of the perturbed solute field. This effectively decreases the length scale for compositional convection, and therefore stabilizes both the boundary and mushy layer modes of convection for $U_\infty < 1000$ (see figure 5). For flows in excess of $U_\infty \approx 1000$ this effect is somewhat reduced at the long wavelengths typical of the mushy layer mode as shown in figure 5. In this case, the vigour of the external flow competes directly with the induced secondary flow, thereby compressing the compositional boundary layer on the upstream faces of the peaks of the perturbed interface. This competition is associated with solutions whose
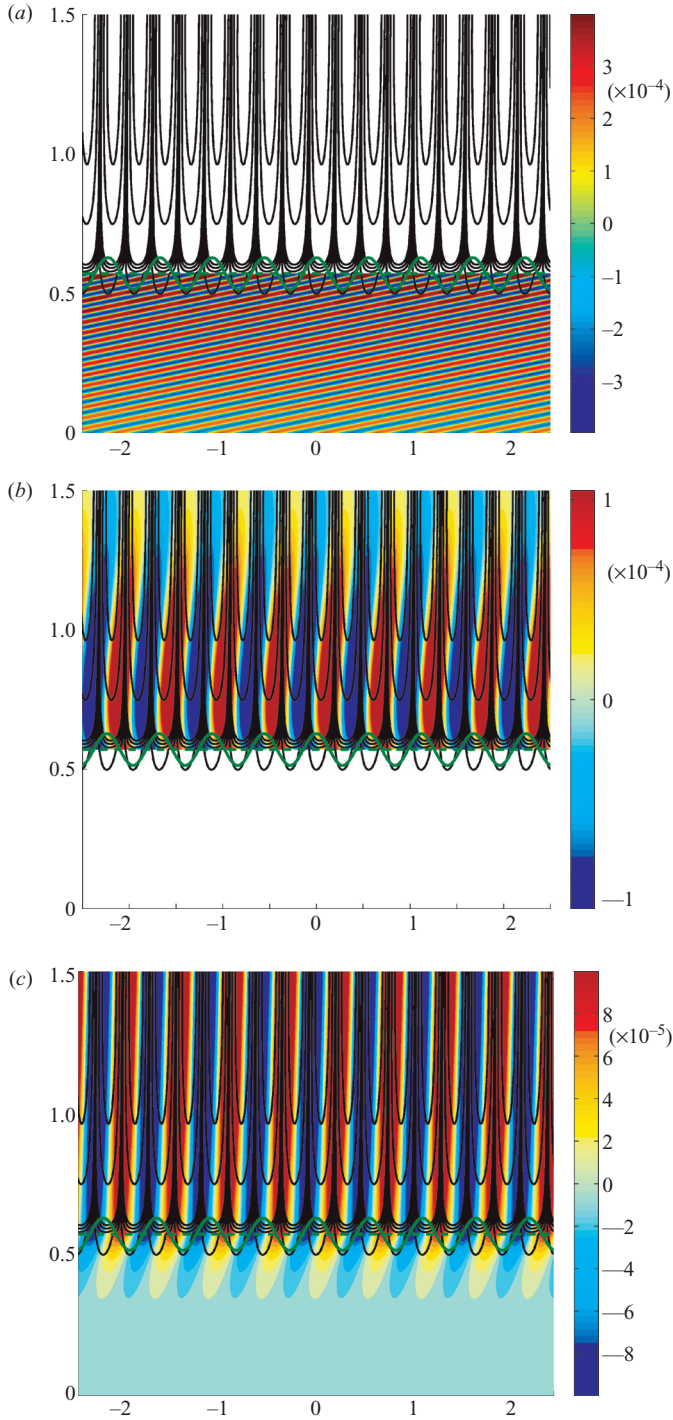
FIGURE 6. The eigenmodes of the forced boundary layer mode for $U_\infty = 3000$, $k = 11.2$, $R_m = 12.6$ and $\sigma_i = -164.6$. Plots are of the streamlines of the flow with (a) the perturbed solid fraction (blue – dissolution, red – solidification), (b) the perturbed concentration (blue – reduced, red – enhanced) and (c) the perturbed thermal field (blue – cooling, red – warming). Thermodynamic parameters are $\mathscr{S} = \mathscr{C} = \theta_\infty = 1$ and the Darcy number is $\Pi_0 = 10^{-5}$.
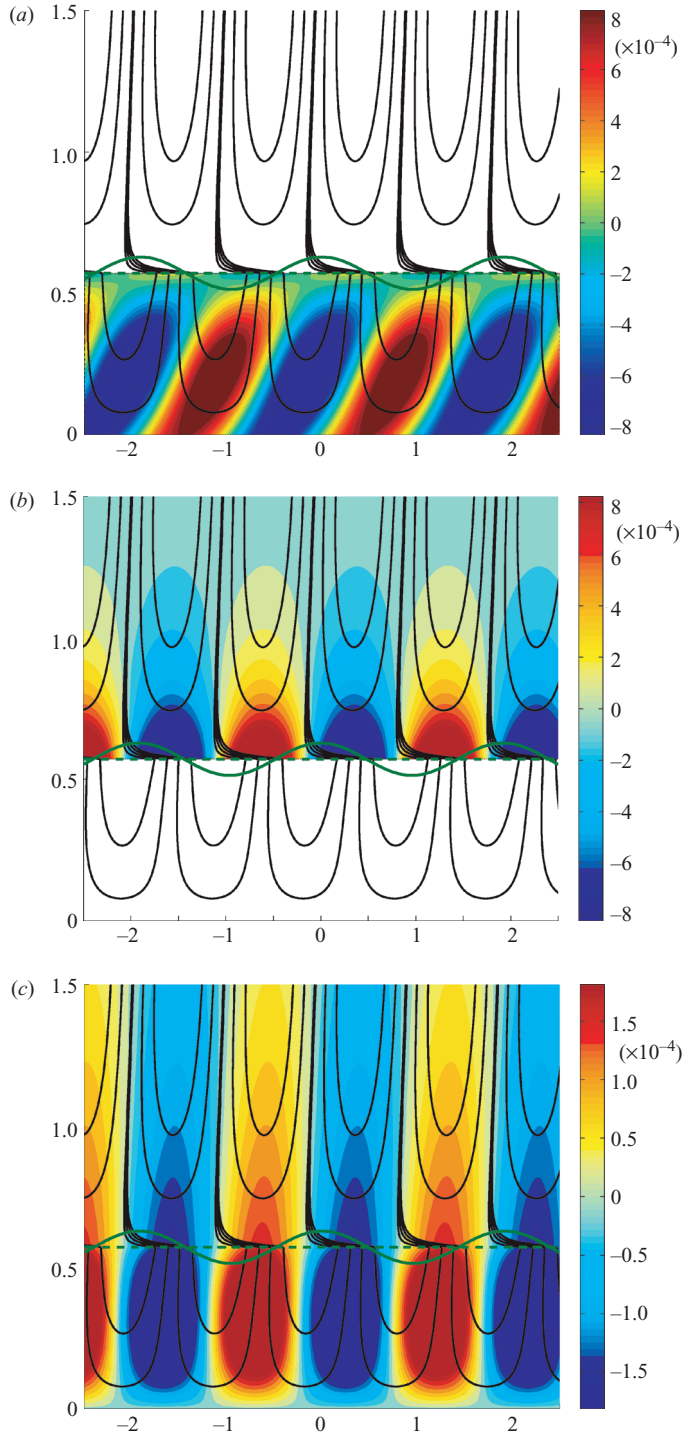
J. A. Neufeld and J. S. Wettlaufer

FIGURE 7. The eigenmodes of the forced mushy layer mode for $U_\infty = 100\,000$, $k = 3.3$, $R_m = 18.1$ and $\sigma_i = -7.7$. Plots are of the streamlines of flow with (*a*) the perturbed solid fraction (blue – dissolution, red – solidification), (*b*) the perturbed concentration (blue – reduced, red – enhanced) and (*c*) the perturbed thermal field (blue – cooling, red – warming). Thermodynamic parameters are $\mathcal{S} = \mathcal{C} = \theta_\infty = 1$ and the Darcy number is $\Pi_0 = 10^{-5}$.
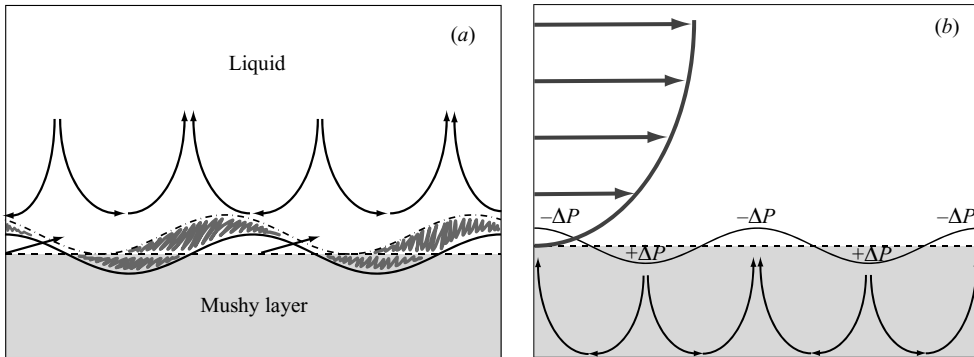
FIGURE 8. The forced boundary layer mode, illustrated in (*a*), occurs when the external flow generates a secondary recirculating flow upwelling on the upstream faces of the peaks as indicated by the curved arrows. This sweeps the compositional boundary layer (shown shaded and bounded by solid and dash-dot lines) from the downstream to the upstream side of the peaks. The resultant decrease (increase) in concentration on the upstream (downstream) face of the peaks generates a growth drive (shown by straight arrows) leading to an interfacial wave which propagates downstream. The forced mushy layer mode, illustrated in (*b*), occurs when the imposed shear flow generates pressure perturbations at the mush–liquid interface which in turn drive circulation within the porous mushy layer. This recirculating flow compresses the isotherms at the peaks leading to growth of the corrugation.

stability is only weakly dependent on the external flow rate for $1000 < U_\infty < 100\,000$. Finally, as the external flow is increased above a critical value ($U_\infty > 2000$ for the boundary layer mode and $U_\infty > 30\,000$ for the mushy layer mode), convection is forced by the external flow. In this regime, the imposition of a parallel shear flow over the interfacial corrugations dominates the secondary flow. At long wavelengths this secondary flow gives rise to negative pressure perturbations at the peaks and positive pressure perturbations at the troughs which in turn drive flow within the mushy layer. Smaller-wavelength corrugations to the mush–liquid interface result in a secondary flow which sweeps the compositional boundary layer upstream. In both cases the consequence is to create a pattern of solidification and dissolution with a planform controlled by the shear.

In detail, we interpret the destabilization of the boundary layer mode as U_∞ becomes large as the instability of a deformable interface in the presence of an external flow. For sufficiently large U_∞ the secondary flow is dominated by the interaction of the corrugated interface with the external flow and as $U_\infty \to U_\infty^c$, $R_m^c \to 0$, in which case buoyancy ceases to play a role and the secondary flow decouples from both thermal and compositional perturbations. In this limit the secondary flow is characterized by upwellings on the upstream faces of interfacial peaks and downwellings on the downstream side with a phase shift of nearly $\pi/2$ from the corrugated interface. Hence, the depletion of solute within the boundary layer associated with growth of the interface and relative enrichment at the troughs is swept upstream by the perturbed flow. This results in preferential growth on the downstream faces of the peaks and dissolution on the upstream faces resulting in a growth which is primarily, but not completely, translational in nature. Thus corrugations to the mush–liquid interface grow and propagate downstream with a phase velocity proportional to the magnitude of the applied shear flow as illustrated schematically in figure 8(*a*). Similar travelling wave solutions have been investigated theoretically by Forth & Wheeler
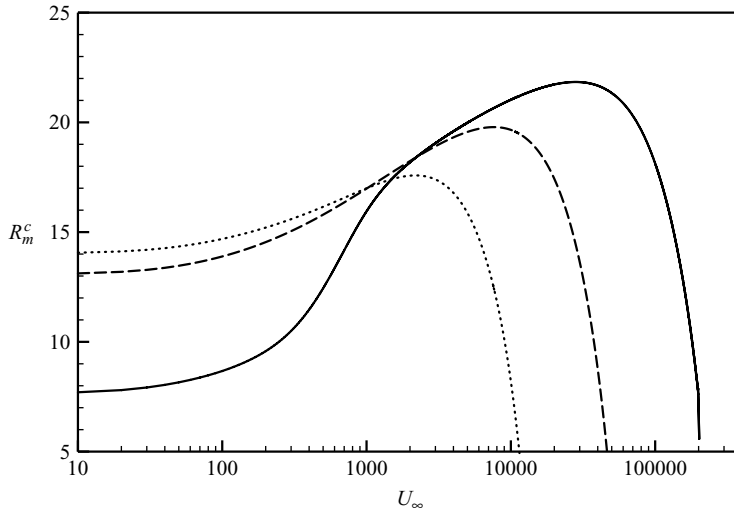
FIGURE 9. Variation of the critical mushy layer mode of instablity, R_m^c, as a function of the permeability. The permeabilities shown are $\Pi_0 = 10^{-5}$ (solid), $\Pi_0 = 10^{-4}$ (dashed) and $\Pi_0 = 10^{-3}$ (dotted) and all curves correspond to the parameter values $\mathscr{C} = \mathscr{S} = \theta_\infty = 1$.

(1989, 1992) in which the effect of shear flows on the Mullins–Sekerka type instability of a solidifying solid–liquid interface were studied. That this effect is not a result of forced flow within the mushy layer can be seen both through the vanishingly small magnitude of flow within the mushy layer as U_∞ becomes large and through the relative insensitivity of the forced mode to changes in the permeability of the underlying mushy layer.

This contrasts with the case of forced mushy layer convection. Here, as first described by Feltham & Worster (1999), the dominant effect of the induced secondary flow is to create negative pressure perturbations at the peaks and positive pressure perturbations at the troughs of the mush–liquid interface as illustrated in figure 8(*b*). The resultant flow within the mushy layer compresses the isotherms at the peaks and rarifies them at the troughs, leading to overall growth of the interfacial corrugation. That this instability is dominated by flow within the mushy layer is clearly demonstrated by the relatively small wave speed associated with compression and rarefaction of the thermal boundary layer within the overlying liquid. More dramatically the dominance of the Darcy number in determining the stability of the forced mushy layer mode attests to the importance of interstitial flow. As shown in figure (9), changing the permeability by one order of magnitude dramatically affects the stability of the system in the presence or absence of an external shear flow. Indeed it is readily apparent that the Bernoulli suction effect is substantially more effective for mushy layers of larger permeability.

In part due to the magnitude of the forced flow associated with the forced mushy layer mode, the consequences for the evolution of the mushy layer are substantial. This Bernoulli-driven motion not only perturbs the isotherms in the mushy layer but, significantly, it drives solidification and dissolution of the matrix. As is the case for the unforced mushy layer mode, this alternate solidification/dissolution pattern is thought to give rise to regions of zero solid fraction within the mushy layer. These patterns, called chimneys, which are cylindrical structures of zero solid fraction within the mushy layer, have been observed by several authors in unforced mushy
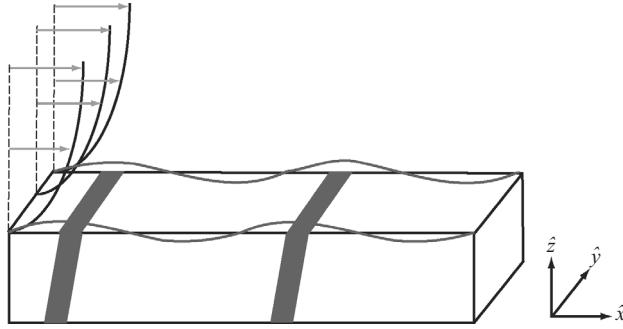
FIGURE 10. Illustration of the planform of crevasses, or grooves (shown in dark shading), regions of zero solid fraction aligned perpendicular to the applied flow, which are the anticipated result of the forced mushy layer mode of convection.

layers, including Copley *et al.* (1970), Chen & Chen (1991), Tait & Jaupart (1992), Wettlaufer *et al.* (1997) and Liu & Hellawell (1999). In contrast, we predict a planform of zero solid fraction crevasses, or grooves, aligned perpendicular to the external flow as illustrated in figure 10. This is the principal influence of the shear flow on the structure of the mushy layer in this regime.

The dependence of the critical Rayleigh number of both the boundary and mushy layer modes of instability shown in figure 5 is typical for a wide range of parameter values. Hence, it is instructive to track the influence of the external shear flow by following the critical value U_∞^c at which $R_m^c = 0$ for both the boundary and mushy layer modes as a function of the thermodynamic parameters (see figure 11). In this limit the effects of buoyancy are absent and both the boundary and mushy layer modes are driven entirely through the interaction of the external flow with the corrugated mush–liquid boundary. The forced boundary layer mode, shown in figure 11(*a*), is driven by redistribution of the compositional boundary layer by the perturbed flow and is therefore relatively insensitive to variations in θ_∞. In contrast both $\mathscr{C}$ and $\mathscr{S}$ characterize the reactivity of the mushy layer to thermal and solutal variations. An increase in $\mathscr{C}$ enhances the solute released upon dissolution, thereby strengthening the basic mechanism leading to the forced boundary layer mode. Similarly, a reduction in $\mathscr{S}$ enhances the amount of the mushy layer that can be dissolved for a given thermal perturbation. Therefore the mush–liquid interface is destabilized by a decrease in $\mathscr{S}$.

Variation of the U_∞^c with the thermodynamic parameters is examined for the forced mushy layer mode in figure 11(*b*). Here it is important to recognize that, as in thermally driven convection, the long-wavelength limit is dominated by diffusion within the mushy layer. Within this reactive porous medium diffusion is modified by solidification and dissolution of the matrix as characterized by the composition ratio $\mathscr{C}$ and the Stefan number $\mathscr{S}$. This is perhaps most clearly illustrated in the limit $\mathscr{C} \gg \theta$ in which case equations (2.5) and (2.6) can be combined to give

$$(\partial_t - \partial_z)\theta + \boldsymbol{u} \cdot \nabla\theta = \frac{\kappa_{\text{eff}}}{\kappa}\nabla^2\theta = \frac{\nabla^2\theta}{1 + \mathscr{S}/\mathscr{C}} \qquad (5.2)$$

as shown by Worster (2000). We note that the effective thermal diffusivity κ_{eff} within this reactive porous medium is therefore enhanced as $\mathscr{C}$ is increased and diminished as $\mathscr{S}$ is increased. This diffusivity acts to smooth out thermal perturbations induced by secondary flow generated by the interaction of the external flow with the corrugated mush–liquid interface, and therefore stabilizes the system. Thus, as $\mathscr{C}$ is increased the
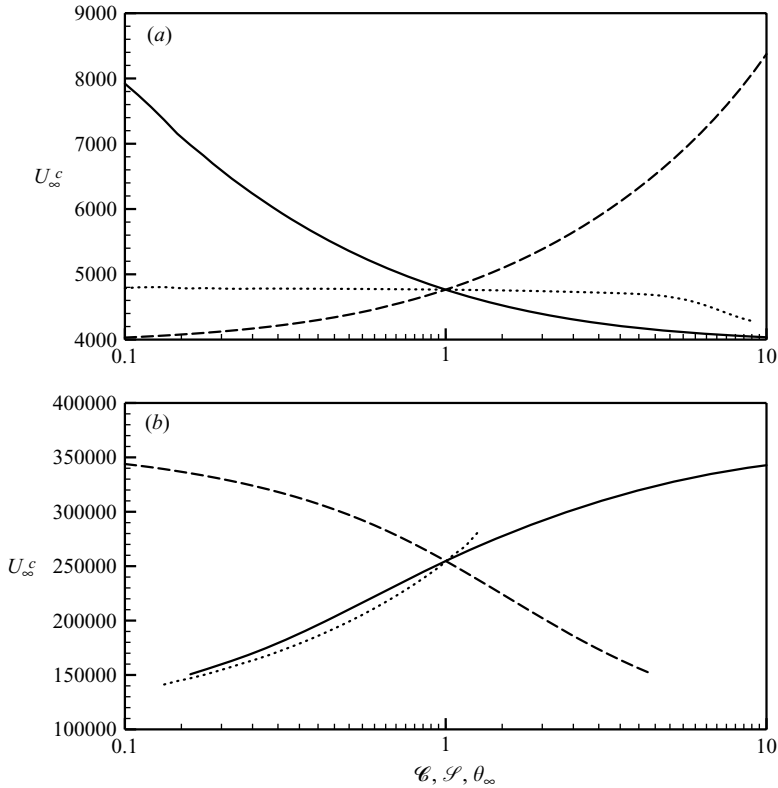
FIGURE 11. Variation of the critical external flow rate, U_∞^c, at which $R_m^c = 0$ as a function of external parameters, $\mathscr{C}$ (solid), $\mathscr{S}$ (dashed), θ_∞ (dotted) for (*a*) the boundary layer mode and (*b*) the mushy layer mode. In each case, one parameter is varied while the remaining parameters are held fixed and equal to unity. See text for discussion.

system is stabilized with respect to the forced mushy layer mode, while an increase in $\mathscr{S}$ destabilizes the system as shown in figure 11(*b*). Finally, we note that the mushy layer depth is decreased as θ_∞ is increased, thereby damping the induced flow within the mushy layer and ultimately leading to stabilization.

5.3. *Comparison with previous work*

The present study complements and extends the work of both Feltham & Worster (1999) and Chung & Chen (2001). Feltham & Worster (1999) studied the effect of a shear flow imposed on a corrugated mushy layer in which the effects of buoyancy were neglected. As noted in the introduction, they found that the perturbed flow in the liquid coupled to flow in the mushy layer through a pressure matching condition creates a Bernoulli suction effect. A critical flow rate was found above which this Bernoulli suction forced flow within the mushy layer on a length scale commensurate with its depth. This fluid motion compresses the isotherms at the peaks and rarefies them at the troughs, resulting in further corrugation of the mush–liquid interface. Chung & Chen (2001) extended this work by including the effects of both compositional and thermal convection, and by coupling flow in the external liquid to flow in the mushy layer through a Beavers–Joseph condition. While they found no appreciable effect on the mushy layer mode they found a critical external shear rate above which the boundary layer mode of convection was forced. They attribute its formation to the

mechanism outlined by Feltham & Worster (1999), namely that pressure perturbations at the mush–liquid interface drive a flow within the underlying mushy layer which is ultimately responsible for the formation of corrugations. In addition, Chung & Chen (2001) report finding a new morphological mode with negative critical Rayleigh number. Their results show that for large enough external shear flows this mode merges with the boundary layer mode.

Here we have examined the effect of a large range of external flows on compositional convection. In contrast to the work of Feltham & Worster (1999) we retain the buoyancy effects leading to natural convection, thereby allowing us to assess the effect of the external shear flow on the boundary and mushy layer modes of convection. Furthermore, by neglecting thermal convection, $R_T = 0$, and by examining the limiting case of small permeability where the Beavers–Joseph condition becomes one of no-slip, we significantly simplify both the mathematical analysis and the interpretation of the resulting stability diagrams. Finally, in contrast to the work of Chung & Chen (2001) we find that both the boundary and mushy layer modes are destabilized above a critical external flow. In addition, we find no evidence for the form of morphological instability described by Chung & Chen (2001). This may be due, in part, to our neglect of thermal contributions to convection since $R_T = 0$ in all our calculations. Our interpretation differs from both these previous studies in the following important respects. First, we find that flow within the mushy layer does not play a role in the shear forced boundary layer mode. Secondly, we find a smooth transition from buoyancy-driven convection to shear-forced convection for both the boundary and mushy layer modes and, as just noted, find no evidence for the morphological mode of Chung & Chen (2001). An immediate consequence of this interpretation is that the two modes greatly differ in their effect on the mushy layer. The effect of the forced boundary layer mode is to generate a travelling interfacial wave, while leaving the structure of the underlying mushy layer relatively unaffected. In contrast to the previous authors, we find that the forced mushy layer mode has the greatest effect on the structure of the mushy layer through solidification and dissolution driven by fluid flow. However, as opposed to the chimneys produced through natural convection we predict that the perturbations typical of this forced mode will give rise to crevasses or grooves of zero solid fraction aligned perpendicular to the external flow because perturbations to the flow field are greatest for wavenumbers aligned with the flow (see figure 10). These predictions are experimentally bourn out by the observations of Neufield & Wettlaufer (2008).

5.4. *Geophysical relevance*

Mushy layers occur in a host of geophysical systems in which shear flows play an important role. In the Earth's polar oceans solidification of sea water, which can be treated as an aqueous sodium chloride solution, can occur in the presence of large-scale oceanic currents. The sea ice which forms is accurately modelled as a mushy layer (see Feltham *et al.* 2006) and is important not only because of its role in the radiation balance of the Earth through the ice–albedo feedback, but also because of its role as a mediator of the heat, mass and momentum fluxes between atmosphere and ocean. Of particular importance are the salt fluxes, which are essential drivers of the thermohaline structure of the polar seas and global deep water masses. The role of oceanic currents in forcing desalination of sea ice can be estimated using the parameters in Feltham & Worster (1999). We find that the forced mushy layer mode can be triggered in sea ice with a dimensional permeability of $\tilde{\Pi}_0 = 10^{-4}$–10^{-7} cm^2, as estimated by Wettlaufer, Worster & Huppert (2000), in the presence of an external

shear flow of magnitude $\tilde{U}_\infty \simeq 10\text{–}800\,\mathrm{cm\,s^{-1}}$. While this shear rate indicates that a reasonably vigorous external current is needed to force mushy layer convection, it does not incorporate macroscopic-scale bottom roughness and should therefore be interpreted as an upper bound. Furthermore, as shown in the present analysis, the efficacy of the forced mushy layer mode of convection is sensitive to the large uncertainties associated with estimates of the dimensional permeability of sea ice. Indeed, while Wettlaufer *et al.* (2000) estimated a more narrow range of *in-situ* depth-averaged permeabilities than used for our estimates here, they noted that these numbers result from field conditions that differ in an important respect from those controlled in the laboratory. Typical laboratory experiments are arranged to capture the classical Stefan-type growth at a fixed cold boundary temperature less than the liquidus. In contrast, when sea ice forms from open water in winter conditions the flux balance that determines the upper (cold) surface temperature is more complex, leading to a transient, slowly cooling, upper boundary temperature. Hence, the depth-averaged solid fraction increases in time causing a slow decrease in the permeability of the ice. The implication for the case of natural sea ice is that under transient shear forcing commonly experienced in the field, the critical conditions necessary to trigger the instability we have analysed herein need be less vigorous early in the evolution of the ice cover. Therefore, horizontal inhomogeneities in the structure, and hence mechanical and thermal properties, of the ice due to this intrinsic dynamic/thermodynamic mechanism of instability may be operative on the large scale. This is particularly relevant under contemporary conditions wherein an increasing fraction of the seasonal ice cover is thin (e.g. Nghiem *et al.* 2007).

6. Conclusion

We have performed a linear stability analysis of the interaction between convection in a solidifying mushy layer and a semi-infinite liquid layer in shear. We find that for a shear rate below a critical value the two modes of buoyancy-driven convection identified by Worster (1992*b*), the boundary layer and mushy layer modes, are moderately suppressed. However, above a critical shear rate the system is unstable to a forced mode of convection. In contrast to the findings of Chung & Chen (2001) we find that for shear flows in excess of a critical value the minimum Rayleigh number of *both* the boundary and mushy layer modes decreases monotonically with increasing U_∞. Perhaps most strikingly, we find that the forced mushy layer mode gives rise regions of zero solid fraction in the form of crevasses, or grooves, which form perpendicular to the applied flow. Furthermore, we find that the permeability of the matrix dominates the mushy layer mode of instability as well as the parameters at which various modes become dominant. Because the permeability is one of the least well-known parameters in most physically relevant systems our results demonstrate the importance of future experiments being focused on determining the permeability under a range of conditions for systems of both metallurgical and geophysical relevance. Such experiments have been initiated by Chen & Chen (1991) and Liu & Hellawell (1999) for the super-eutectic aqueous ammonium chloride system. Moreover, the analysis presented here would need to be modified in the nonlinear regime to correctly deal with the increasing permeability, and hence the relevance of the Beavers–Joseph conditions, as the instability evolves.

The physical mechanisms investigated here may be important in a whole host of geophysical and industrial settings. For example, in the polar oceans, salt and turbulent fluxes are dominated by the formation of young sea ice. As we have shown,

oceanic shear flows may significantly alter the nature of these fluxes and hence the structure of the sea ice. Finally, the physical mechanism outlined above indicates the possibility of tailoring external flows to manipulate the solidification patterns of dendritic networks – a major goal in materials science.

Appendix. Asymptotic treatment of the liquid region

Owing to a regular singularity in the liquid equations at $s = 0$ we match asymptotic solutions for the variables as $s \to 0$. The asymptotics are most clearly enumerated by defining

$$(\theta_1, \Theta_1, \Omega_1, w_1) = \sum_{j=1}^{4} s^{m_j}(\tilde{\theta}_j, \tilde{\Theta}_j, \tilde{\Omega}_j, \tilde{w}_j) \tag{A1}$$

and hence equations (4.14)–(4.17) become

$$\left[s^2 D_s^2 + 2m_j s D_s + m_j^2 - m_j - k^2 - i\sigma_i \right] \tilde{\theta}_j = ikU_\infty \left(1 - s^{1/Pr} \right) \tilde{\theta}_j + (\theta_\infty - \theta_i) s \tilde{w}_j, \tag{A2}$$

$$\left[\epsilon s^2 D_s^2 + (2m_j \epsilon + \epsilon - 1) s D_s + \epsilon m_j^2 - m_j - \epsilon k^2 - i\sigma_i \right] \tilde{\Theta}_j$$
$$= ikU_\infty \left(1 - s^{1/Pr} \right) \tilde{\Theta}_j - (\theta_i/\epsilon) s^{1/\epsilon} \tilde{w}_j, \tag{A3}$$

$$\left[Pr s^2 D_s^2 + (2m_j Pr + Pr - 1) s D_s + Pr m_j^2 - m_j - Pr k^2 - i\sigma_i \right] \tilde{\Omega}_j$$
$$= ikU_\infty \left[\left(1 - s^{1/Pr} \right) \tilde{\Omega}_j + Pr^{-2} s^{1/Pr} \tilde{w}_j \right] + k^2 Pr(R_T \tilde{\theta}_j - R_C \tilde{\Theta}_j), \tag{A4}$$

$$\left[s^2 D_s^2 + (2m_j + 1) s D_s + m_j^2 - k^2 \right] \tilde{w}_j = \tilde{\Omega}_j. \tag{A5}$$

The resultant four linearly independent solutions are of the form

i	$\tilde{\theta}_j$	$\tilde{\Theta}_j$	$\tilde{\Omega}_j$	$\tilde{w}_j$
1	1	0	$\dfrac{Pr k^2 R_T}{Pr m_j^2 - m_j - Pr k^2 - i(kU_\infty + \sigma_i)}$	$\dfrac{Pr k^2 R_T}{\left[m_j^2 - k^2 \right]\left[Pr m_j^2 - m_j - Pr k^2 - i(kU_\infty + \sigma_i) \right]}$
2	0	1	$\dfrac{-Pr k^2 R_C}{Pr m_j^2 - m_j - Pr k^2 - i(kU_\infty + \sigma_i)}$	$\dfrac{-Pr k^2 R_C}{\left[m_j^2 - k^2 \right]\left[Pr m_j^2 - m_j - Pr k^2 - i(kU_\infty + \sigma_i) \right]}$
3	0	0	1	$\dfrac{1}{m_j^2 - k^2}$
4	0	0	0	1

$$\tag{A6}$$

where

$$m_1 = \frac{1}{2}[1 + \sqrt{1 + 4k^2 + 4\mathrm{i}(kU_\infty + \sigma_i)}], \tag{A7a}$$

$$m_2 = \frac{1}{2\epsilon}[1 + \sqrt{1 + 4\epsilon^2 k^2 + 4\epsilon\mathrm{i}(kU_\infty + \sigma_i)}], \tag{A7b}$$

$$m_3 = \frac{1}{2Pr}[1 + \sqrt{1 + 4Pr^2 k^2 + 4Pr\mathrm{i}(kU_\infty + \sigma_i)}], \tag{A7c}$$

$$m_4 = k. \tag{A7d}$$

The first and second derivatives are then given by

$$\mathrm{D}_s\tilde{\theta}_j = \frac{(\theta_\infty - \theta_i)\tilde{w}_j}{m_j^2 + m_j - k^2 - \mathrm{i}(kU_\infty + \sigma_i)}, \tag{A8a}$$

$$\mathrm{D}_s\tilde{\Theta}_j = 0, \tag{A8b}$$

$$\mathrm{D}_s\tilde{\Omega}_j = \frac{Prk^2 R_T \mathrm{D}_s\tilde{\theta}_j}{Prm_j^2 + m_j(2Pr - 1) + Pr - 1 - Prk^2 - \mathrm{i}(kU_\infty + \sigma_i)}, \tag{A8c}$$

$$\mathrm{D}_s\tilde{w}_j = \frac{\mathrm{D}_s\tilde{\Omega}_j}{m_j^2 + 2m_j + 1 - k^2}, \tag{A8d}$$

$$\mathrm{D}_s^2\tilde{\theta}_j = \frac{2(\theta_\infty - \theta_i)\mathrm{D}_s\tilde{w}_j}{m_j^2 + 3m_j + 2 - k^2 - \mathrm{i}(kU_\infty + \sigma_i)}, \tag{A8e}$$

$$\mathrm{D}_s^2\tilde{\Theta}_j = 0, \tag{A8f}$$

$$\mathrm{D}_s^2\tilde{\Omega}_j = \frac{Prk^2 R_T \mathrm{D}_s^2\tilde{\theta}_j}{Prm_j^2 + m_j(4Pr - 1) + 4Pr - 2 - Prk^2 - \mathrm{i}(kU_\infty + \sigma_i)}, \tag{A8g}$$

$$\mathrm{D}_s^2\tilde{w}_j = \frac{\mathrm{D}_s^2\tilde{\Omega}_j}{m_j^2 + 4m_j + 4 - k^2}. \tag{A8h}$$

REFERENCES

ACHER, U. M., MATTHEIJ, R. M. M. & RUSSELL, R. D. 1987 *Numerical Solution of Boundary Value Problems for Ordinary Differential Equations*. Classics in Applied Mathematics, vol. 23. SIAM.

BEAVERS, G. S. & JOSEPH, D. D. 1967 Boundary conditions at a naturally permeable wall. *J. Fluid Mech.* **30** (1), 197–207.

CHEN, C. F. & CHEN, F. 1991 Experimental study of directional solidification of aqueous ammonium chloride solution. *J. Fluid Mech.* **227**, 567–586.

CHEN, F., LU, J. W. & YANG, T. L. 1994 Conective instability in ammonium chloride solution directionally solidified from below. *J. Fluid Mech.* **276**, 163–187.

CHUNG, C. A. & CHEN, F. 2001 Morphological instability in a directionally solidifying binary solution with an imposed shear flow. *J. Fluid Mech.* **436**, 85–106.

COPLEY, S. M., GIAMEI, A. F., JOHNSON, S. M. & HORNBECKER, M. F. 1970 The origin of freckles in binary alloys. *IMA J. Appl. Maths* **35**, 159–174.

DAVIS, S. H. 1990 Hydrodynamic interactions in directional solidification. *J. Fluid Mech.* **212**, 241–262.

DAVIS, S. H. 2001 *Theory of Solidification*. Cambridge University Press.

FELTHAM, D. L., UNTERSTEINER, N., WETTLAUFER, J. S. & WORSTER, M. G. 2006 Sea ice is a mushy layer. *Geophys. Res. Lett.* **33**, L14501.

FELTHAM, D. L. & WORSTER, M. G. 1999 Flow-induced morphological instability of a mushy layer. *J. Fluid Mech.* **391**, 337–357.

FELTHAM, D. L., WORSTER, M. G. & WETTLAUFER, J. S. 2002 The influence of ocean flow on newly forming sea ice. *J. Geophys. Res.* **107** (C2), 3009.

FORTH, S. A. & WHEELER, A. A. 1989 Hydrodynamic and morphological stability of the unidirectional solidification of a freezing binary alloy: a simple model. *J. Fluid Mech.* **202**, 339–366.

FORTH, S. A. & WHEELER, A. A. 1992 Coupled convective and morphological instability in a simple model of the solidification of a binary alloy, including a shear flow. *J. Fluid Mech.* **236**, 61–94.

GLICKSMAN, M. E., CORIELL, S. R. & MCFADDEN, G. B. 1986 Interaction of flows with the crystal-melt interface. *Annu. Rev. Fluid Mech.* **18**, 307–335.

HILLS, R. N., LOPER, D. E. & ROBERTS, P. H. 1983 A thermodynamically consistent model of a mushy zone. *Q. J. Mech. Appl. Maths* **36** (4), 505–539.

KELLER, H. B. 1976 *Numerical Methods for Two-Point Boundary-Value Problems*. SIAM.

LIU, S. & HELLAWELL, A. 1999 Experiments with constrained chimney-plume flows in the system ammonium-chloride water: comparison with the unconstrained case. *J. Fluid Mech.* **388**, 21–48.

MORISON, J. H. & MCPHEE, M. 2001 *Encyclopedia of Ocean Sciences*, chap. 3. *Ice-Ocean Interaction*, pp. 1271–1281. Academic.

MULLINS, W. W. & SEKERKA, R. F. 1964 Stability of a planar interface during solidification of a dilute binary alloy. *J. Appl. Phys.* **35** (2), 444–451.

NEUFELD, J. A. & WETTLAUFER, J. S. 2008 An experimental study of shear-enhanced convection in a mushy layer. *J. Fluid Mech.* **612**, 363–385.

NEUFELD, J. A., WETTLAUFER, J. S., FELTHAM, D. L. & WORSTER, M. G. 2006 Corrigendum to flow-induced morphological instability of a mushy layer. *J. Fluid Mech.* **549**, 442–443.

NGHIEM, S. V., RIGOR, I. G., PEROVICH, D. K., CLEMENTE-COLÓN, P. & WEATHERLY, J. W. 2007 Rapid reduction of Arctic perennial sea ice. *Geophys. Res. Lett.* **34**, LI9504.

PRESS, W. H., TEUKOLSKY, S. A., VETTERLING, W. T. & FLANNERY, B. P. 1997 *Numerical Recipes in Fortran 77: The Art of Scientific Computing*, 2nd edn. Cambridge University Press.

TAIT, S. & JAUPART, C. 1992 Compositional convection in a reactive crystalline mush and melt differentiation. *J. Geophys. Res.* **97** (B5), 6735–6756.

WELLS, M. G. & WETTLAUFER, J. S. 2007 The long-term circulation driven by density currents in a two-layer stratified basin. *J. Fluid Mech.* **572**, 37–58.

WETTLAUFER, J. S., WORSTER, M. G. & HUPPERT, H. E. 1997 Natural convection during solidification of an alloy from above with application to the evolution of sea ice. *J. Fluid Mech.* **344**, 291–316.

WETTLAUFER, J. S., WORSTER, M. G. & HUPPERT, H. E. 2000 Solidification of leads: Theory, experiment, and field observations. *J. Geophys. Res.* **105** (C1), 1123–1134.

WORSTER, M. G. 1986 Solidification of an alloy from a cooled boundary. *J. Fluid Mech.* **167**, 481–501.

WORSTER, M. G. 1992a The dynamics of mushy layers. In *Interactive dynamics of convection and solidification* (ed. S. H. Davis, H. E. Huppert, W. Müller & M. G. Worster), pp. 113–138. Kluwer.

WORSTER, M. G. 1992b Instabilities of the liquid and mushy regions during solidification of alloys. *J. Fluid Mech.* **237**, 649–669.

WORSTER, M. G. 1997 Convection in mushy layers. *Annu. Revi. Fluid Mech.* **29**, 91–122.

WORSTER, M. G. 2000 Solidification of fluids. In *Perspectives in Fluid Dynamics: A Collective Introduction to Current Research*, chap. *Solidification of Fluids* (ed. G. K. Batchelor, H. K. Moffatt & M. G. Worster), pp. 393–446. Cambridge University Press.